Direct measurement of normal and shear forces between surface-grown polyelectrolyte layers

Iain E. Dunlop[1,4,], Wuge H. Briscoe[1], Simon Titmuss[1], Robert M.J. Jacobs[1], Vicky L. Osborne[2,5], Steve Edmondson[2,6], Wilhelm T.S. Huck[2] and Jacob Klein[1,3,*]*

[1] Department of Chemistry, University of Oxford, South Parks Road, Oxford, OX1 3QZ, U.K., [2] Melville Laboratory for Polymer Synthesis, University Chemistry Laboratory, Lensfield Road, Cambridge, CB2 1EW, U.K., [3] Department of Materials and Interfaces, Weizmann Institute of Science, PO Box 26, Rehovot 76100, Israel, [4] Present address: Dept. New Materials and Biosystems, Max Planck Institute for Metals Research, Heisenbergstraße 3, 70569 Stuttgart, Germany, [5] Present address: Department of Colour Science, University of Leeds, Leeds, LS2 9JT, U.K., [6] Present address: Department of Chemistry, University of Sheffield, Brook Hill, Sheffield, S3 7HF, U.K.

* To whom correspondence should be addressed: dunlop@mf.mpg.de, jacob.klein@chem.ox.ac.uk.

Abstract

This paper presents measurements, using the surface force balance (SFB), of the normal and shear forces in aqueous solutions between polyelectrolyte layers grown directly on mica substrates (grafted-from). The grafting-from was via surface-initiated atom transfer radical polymerization (surface-initiated ATRP) using a positively-charged methacrylate monomer. X-ray reflectometry measurements confim the successful formation of polyelectrolyte layers by this method. Surface-inititated ATRP has the advantages that the polymer chains can be strongly grafted to the substrate, and that high grafting densities should be achievable. Measured normal forces in water showed a long-range repulsion arising from an electrical double layer that extended beyond the polyelectrolyte layers, and a stronger, shorter-range repulsion when the polyelectrolyte brushes were in contact. Swollen layer thicknesses were in the range 15 – 40 nm. Upon addition of ~10^{-2} M – 10^{-1} M sodium nitrate, screening effects reduced the electrical double layer force to an undetectable level. Shear force measurements in pure water were performed, and the measured friction may arise from polymer chains bridging between the surfaces.

Introduction

Measurements of the frictional forces between neutral polymer brushes have shown them to have remarkable lubricating properties [1-4]. These properties have been attributed to the very limited interpenetration between opposing polymer brushes even at quite high compressions suggested by some theoretical studies [5-7]. Additionally, it has been suggested that polymer brushes may play lubricating roles in certain biological contexts where cells bearing surface-grafted polymers side past one another, such as in articular cartilage [8] and at the ocular surface [9-12]. Most relevant studies of polymer friction were carried out on neutral polymer brushes [2, 13-16], with a few recent exceptions [17-20]. However, since surface-active biological polymers are typically electrically charged, biological lubrication would be better modeled by studying polyelectrolyte brushes. The presence of electrical charge could influence the friction by two mechanisms: firstly, electrical charge affects brush structure and may reduce the degree of interpenetration between opposing brushes [21], and secondly it has been suggested that bound hydration layers around charged groups can have a lubricating effect [22, 23].

Some previous surface force balance (SFB) studies of polyelectrolyte brushes have used brushes formed from diblock copolymers [17, 24-26]. In particular, the friction between polyelectrolyte brushes has been studied using a system of diblock copolymers adsorbed to a hydrophobized mica surface via a hydrophobic block, with a block bearing negatively-charged carboxylate groups forming the brush [17]. At moderate compressions the friction coefficient between such brushes was lower than that between either neutral polymer brushes or layers of adsorbed polyelectrolyte at comparable volume fractions. However, the brush was not stable under shear at high compressions, due to the relatively weak nature of the physical bonds between the diblocks and the surface. This is a disadvantage of most brushes formed from diblock copolymers, although this problem has recently been addressed by Liberelle and Giasson, who measured the friction between polyelectrolyte brushes formed from diblock copolymers, where the hydrophobic anchoring blocks were entangled with a preexisting

polymer layer, giving a stronger bond to the mica surface [20]. A second disadvantage, which applies not only to diblock copolymers but to any method whereby brushes are formed by self-assembly from preexisting polymers in solution – so-called *grafting-to* approaches – is that the maximum brush density that can be produced by grafting-to is kinetically limited [27-29]. This limitation arises from the fact that for a new chain to join the brush, its surface-active part must diffuse through the energy barrier created by the preexisting partially-formed brush. The magnitude of this barrier increases progressively with increasing brush density, so that the formation of high density brushes can take an impracticably long time.

Polymer layers that are synthesized directly from the surface – so-called *grafted-from* layers – can avoid both the above disadvantages of diblock copolymer layers; high density layers that are strongly grafted to the surface can be produced [30]. Polymer layers that are synthesized from the surface are typically produced by first functionalizing the substrate with a self-assembled coating of small molecules bearing polymerization initiator groups. The functionalized substrate is then incubated in a solution of monomer, and polymer chains grow out from the initiator sites. The polymer layer will be as strongly bound to the surface as the self-assembled monolayer on which it is grown, and the polymer layer density is not strongly kinetically limited, as only small monomer (and maybe catalyst) molecules need to diffuse through the partially formed polymer layer.

In this paper, we synthesized grafted-from polyelectrolyte layers from a surface using atom transfer radical polymerization (ATRP), which has become popular for the synthesis of polymers with complex, well-defined architectures (for an introduction see Matyjazewski [31]). ATRP is a method of carrying out free radical polymerization that minimizes unwanted reactions between adjacent chains and thus allows good molecular weight control. ATRP was first used to synthesize brushes by Ejaz *et al.* [32]; for reviews of recent work, see Pyun *et al.* [33] Edmondson *et al.* [34], Rühe *et al.* [35] and Ballauff and Borisov [36]. Due to the versatility of ATRP, the experimental method described in this paper should be readily adaptable to permit SFB

studies of polymers that have been synthesized from a surface with a wide variety of functionalities and architectures.

In order to synthesize a polymer brush by ATRP, it is necessary to first anchor molecules bearing initiator functional groups to the surface. For silicon oxide surfaces, an initiator molecule bearing a trifunctional silane has been used to form a self-assembled monolayer that is stabilized both by covalent bonding to the surface and by crosslinking [37]. Indeed, this method has been used to perform an SFB experiment using neutral polymer brushes on a glass substrate [38]. The traditional mica substrate for SFB is, however, preferable, since it can readily be cleaved into symmetric sheets for more accurate separation measurements. Stable silane monolayers can be formed on mica that has been pretreated with a water plasma to introduce pendant –OH bonds [39]. This method has been used in the context of SFB experiments to hydrophobize mica surfaces [39-41] and its plausibility as a method of covalently anchoring large molecules has been demonstrated in a study of protein immobilization [42]. The covalent attachment of a silane-functionalized ATRP initiator to water plasma-treated mica surfaces, and the growth of a polymer layer from the surface, has recently been reported [43]. In this paper, we have anchored trifunctional silane ATRP initiator molecules to a water plasma-treated mica surface as a prelude to synthesizing polyelectrolyte layers from that surface for SFB experiments. The polyelectrolyte layer was synthesized using the well-known acrylate ATRP method, and the monomer, 2-(methacryoyloxy)ethyl]trimethylammonium chloride (METAC) (structure in figure 1a), consists of a methacrylate to which a strong electrolyte group in the form of a quaternary ammonium chloride has been attached, so that the polymer chains are strongly positively charged in water. We have performed SFB measurements of normal and shear forces between the polyelectrolyte layers, characterizing the repulsive forces between the surfaces, the hysteresis when the surfaces are brought together and pulled apart, and the frictional force between the surfaces at high compressions.

The poly(METAC) layers used in this study differ from the classical idea of a polyelectrolyte brush, in that the positively-charged polyelectrolyte chains are likely to experience both electrostatic and hydrophobic attractions to the initiator-coated substrate surface (the latter arising from surface attachment of hydrophobic groups on the chain backbone), which may well retain some of the negative charge of the original mica. However, the normal forces between the polyelectrolyte layers strongly resemble those between brushes where there is no polyelectrolyte-surface attraction (see 'Results and Discussion'). This may be understood with reference to the theoretical work of Zhulina *et al.* [44], who found that, for sufficiently large amounts of polyelectrolyte per unit area, polyelectrolyte molecules end-grafted to oppositely-charged surfaces form a two-layer structure, with some polyelectrolyte adsorbed tightly to the surface, reversing the effective surface charge. The remaining polyelectrolyte chains stretch away from the now effectively like-charged surface, forming a classical polyelectrolyte brush. Surface-grown poly(METAC) layers have recently been observed to form such two-layer structures in neutron reflectometry studies carried out using initiator-coated sapphire substrates which were hydrophobic (although not negatively charged) [45].

The normal forces between polyelectrolyte layers that adopt two-layer structures as postulated by Zhulina *et al.* should be similar to those between polyelectrolyte brushes on nonattractive surfaces, with the addition of a force arising when the compression of the brush layer causes additional polyelectrolyte molecules to adsorb to the surface, which will be hysteretic except at long timescales. It will be seen below that the normal forces between the poly(METAC) layers in this study do indeed show some hysteresis, the magnitude of which is however much less than that of the total repulsive force, so that it is appropriate to a first approximation to model the normal forces using theoretical ideas developed for non-adsorbing polyelectrolyte brushes. In contrast, it will be seen that polyelectrolyte-substrate attractions may have a dominant effect on the shear forces between the poly(METAC) layers. In the

remainder of this paper, we will refer to the surface-grown poly(METAC) layers as 'brushes', but the likelihood of attractive polymer-substrate interactions should be borne in mind.

Experimental section

Surface-grown polyelectrolyte layers

Initiator-functionalization of mica surfaces

Mica substrates were prepared for polyelectrolyte brush growth by functionalization with initiator groups, as follows. Freshly-cleaved mica surfaces were treated with an Ar/H_2O plasma for 2 mins at 6.8 W radio frequency power (Harrick Basic Plasma Cleaner, Harrick Scientific Coorporation, Pleasantville, N.Y., U.S.A.), to introduce –OH groups to the mica surface and thus enable covalent attachment of methoxysilane molecules [37, 43]. The mica surfaces were then reacted with silane initiator in the vapor phase, to avoid the possibility of surface contamination by polymerized particles that exists when silane layers are deposited from solution (shown by unpublished atomic force microscopy studies of (3-aminopropyl)trimethoxysilane monolayers on silica substrates). The surfaces were placed in a 2 l vacuum dessicator that also contained a beaker containing a solution of silane initiator, 3-trimethoxysilylpropyl-2-bromo-2-methylpropionate (structure in figure 1b, 0.25 g) in anhydrous hexane. Silane initiator (custom synthesized by Gelest Inc., Morrisville, P.A., U.S.A.) was supplied as a liquid in 0.25 g aliquots in flame-sealed glass ampoules, refrigerated, and used within one year of receipt; no cloudiness was visible in these aliquots, suggesting that these precautions against silane polymerization were successful. The dessicator was pumped out for 5 minutes (Divac 0.6L pump with PTFE diaphragm from Leybold Vacuum, Germany, pump minimum pressure $\leq$ 8 mbar), sealed for a chosen incubation time which was 1 hour in the case of the SFB experiments and then vented.

Atom transfer radical polymerization (ATRP)

[2-(methacryoyloxy)ethyl]trimethylammonium chloride (METAC, structure in figure 1a) can be polymerized using the copper/2,2'-dipyridine catalyst system commonly used for

acrylate ATRP. The polymerization protocol used in this study was based on that of Osborne *et al.* [46] However, this protocol uses a methanol-water mixture, which attacks the Shell Epon-1004 glue that is traditionally used in aqueous mica SFB experiments, as the reaction solvent; it was therefore desirable to use a pure water solvent. Naive implementation of the procedure of Osborne *et al* [46] with a pure water solvent resulted in a brush that terminated almost immediately, and could not thus be grown to a significant thickness (as measured using ellipsometry in ambient air (Picometer Elliposometer, Beaglehole Instruments, Wellington, New Zealand) on a dry brush grown on an initiated silicon wafer). This result was to be expected, since ATRP in aqueous solution in the absence of alcohols tends to become rapid and uncontrolled, due to the instability of the controlling copper complexes [47]. In order to counteract this effect, a large excess of deactivating copper (II) chloride was used, and N,N'-Bis[2-(dimethylamino)ethyl]-N,N'-dimethylethane-1,2-diamine (HMTETA) was used as the ligand to solubilize the copper ions, rather than the 2,2'-dipyridine used by Osborne *et al.* [46]. Under these conditions, a brush of satisfactory thickness, as used in the SFB experiments could be grown in 15 minutes, giving the additional benefit that the polymerization could be carried out under ambient air rather than under an inert atmosphere, since termination due to ambient oxygen did not have time to occur.

The detailed procedure for brush growth in SFB experiments was as follows. METAC solution (75 g of 75 wt.-% in water, Sigma-Aldrich U.K.) was mixed with 75 ml ultrapure water (purified by a Rios 5 – Gradient A10 system, Millipore Corp., Billarica, M.A., U.S.A.). Aqueous sodium hydroxide and hydrochloric acid were added dropwise to adjust the solution to pH 8.00 ± 0.15 (determined by using a pH meter to measure removed aliquots). To 50 ml of the resulting solution was added HMTETA (0.5 ml), copper (I) chloride (anhydrous, 0.036 g) and copper (II) chloride (anhydrous, 0.22 g), giving a molar copper (I) chloride to copper (II) chloride ratio of 2:9. The solution was stirred for around 15 minutes, then the initiator-functionalized mica surface was incubated in it for 15 minutes. The mica (mounted on its

cylindrical lenses) was then removed, rinsed with ultrapure water, and immediately returned to the SFB and submerged in water.

Samples for X-ray reflectometry measurements were prepared in a similar way, although on larger mica sheets rather than lens-mounted surfaces, but were blown dry with dry N_2 immediately after being rinsed with ultrapure water.

Specular X-ray reflectometry

Laboratory-based X-ray reflectometry (Bruker D8 Advance Reflectometer, Bruker AXS Inc., Madison, W.I., U.S.A., with a home-built sample stage, Cu Kα X-rays) was used to characterize 'dry' poly(METAC) brushes prepared as above. Film thicknesses were determined by fitting the reflectivity as a function of momentum transfer $q = \frac{4\pi}{\lambda}\sin 2\theta$, where λ is the X-ray wavelength and θ is the angle between the X-ray beam and the plane of the surface, using the Parratt algorithm [48] (Parrat32 software, Hahn-Meitner Institute, Berlin, Germany [49]). Clear Kiessig (interference) fringes were observed, giving confidence in the values obtained.

Surface force balance (SFB)

The SFB technique has been described in detail elsewhere [50]. Briefly, two pieces of mica of identical thickness in the range 1-5 μm and about 1 cm × 1 cm in area are half-silvered on one side, glued (Epon-1004 epoxy resin from Shell U.K., Ltd.) – silver side down – onto transparent silica cylindrical lenses and placed in the SFB, facing each other with their cylindrical axes crossed. The distance between the two silver layers is measured using white light multiple beam interference, and the distance, *D,* between the mica front surfaces can be inferred from this after calibration of the mica thickness. In this paper, the distance resolution was about ± 0.5 nm; resolution as high as ± (0.1 – 0.2) nm can be obtained if required. The purpose of the SFB is to measure the interaction force as a function of surface separation, *D*. The surfaces can be driven together or apart, using a mechanical drive or a piezoelectric

crystal. One surface is mounted on a spring: the deflection of the spring gives the normal force between the two surfaces. The normal force resolution depends on the spring constant, and was typically ± 0.1 μN. The measured normal force between the two cylindrical mica surfaces, *F(D)*, can be related to the interaction free energy per unit area between two parallel plates, *W(D)*, via the Derjaguin approximation [51]

$$F(D) = 2\pi(R_1R_2)^{1/2}W(D), \qquad (1)$$

where R_1, R_2 are the radii of curvature of the crossed cylinders.

In addition to normal force measurements, we will also present measurements of the shear force between the surfaces. A sectored piezoelectric crystal is used to drive the top surface, which is connected to the SFB housing via a lateral spring, in a direction parallel to the bottom surface, which cannot move laterally. If there is a shear force between the surfaces, the lateral spring deflects, and this deflection is measured by an airgap capacitor (Accumeasure, MTI Instruments Inc., Albany, N.Y., U.S.A.). The shear force is the product of the measured deflection with the known spring constant of the lateral spring. The shear force resolution is limited by mechanical noise, and in this paper was around ± 4 μN. (A resolution as good as ± 20 nN can be obtained optimally by reducing mechanical noise and using digital signal filtering [52].)

Procedure

To ensure freedom from particulate contamination, all preparations were carried out in a laminar flow cabinet. Glassware was cleaned using a mixture of hydrogen peroxide and sulfuric acid in roughly 1:3 ratio, rinsed with ultrapure water then ethanol, and blown dry with N_2. Stainless steel parts, and the PTFE tubes used to inject fluids into the SFB, were incubated in 30% nitric acid at 60-80 ºC for around half an hour before being similarly rinsed and dried. Gas-tight syringes (Hamilton Company, Reno, N.V., U.S.A.) used for fluid injection were cleaned with a Tipcleaner (BioForce Nanosciences Inc., Ames, I.A., U.S.A.)

The mica pieces used in this study were obtained by cutting the cleaved mica with a heated platinum wire. It has been observed that this method can contaminate the surfaces with platinum nanoparticles [53], however in this study the mica was always held upstream of the platinum wire in the laminar flow. This method of cutting has been shown to produce surfaces that are free from platinum nanoparticles, except very near the edges where the surfaces are not used [54], and to produce results in SFB experiments that are identical to those produced using mica prepared without hot wire cutting [55].

Immediately after the mica surfaces had been glued to the silica lenses, they were mounted in the SFB and brought into contact in dry air to establish that they were free from contamination and to determine the zero of surface separation. The surfaces were then dismounted, surface functionalization was carried out, and the surfaces were remounted in the SFB, whereupon measurements were carried out. This procedure introduced an error of typically ± 0.5 nm into the zero of surface separation, since it was difficult to control precisely the relative orientation of the mica sheets on remounting.

Results and discussion

Characterization of initiator layer and brush growth

Figure 2a shows the X-ray reflectivity, R, as a function of momentum transfer, q, from a silane-initiator-functionalized mica substrate. Due to the presence of a visible Kiessig fringe arising from interference between reflection at the top and bottom interfaces, the thickness of the initiator layer can be determined as described in the 'Experimental section'. This gives a value of 10.5 ± 1.0 Å, consistent with the structure of the initiator molecule [56].

When poly(METAC) layers were grown on initiator-functionalized mica substrates and then blown dry, their X-ray reflectivity profiles showed Kiessig fringes whose spacing was much lower than for an initiator-only substrate (figure 2b shows a typical example), confirming that poly(METAC) growth had occurred. The layer thickness can be used to determine the amount of poly(METAC) per unit area, Γ_{poly}, since the poly(METAC) layers are likely to contain

around 86% water, as deduced from neutron reflectometry measurements on a similar poly(METAC) layer on a sapphire substrate [45]. The measured X-ray reflectometry profiles also confirmed that mica substrates were uniformly covered by the poly(METAC) layers, since the electron density values obtained by fitting were equal within the scatter to that expected for a continuous film of poly(METAC) and water, rather than the lower value that would have been given by an incomplete layer.

As a control experiment to confirm that the observed layers were indeed formed by ATRP, a sample was prepared using a much higher ratio of copper (II) to copper (I) than usual, with the aim of almost completely suppressing polymer growth by ATRP, while leaving other conditions unchanged [57]. The layer thickness, including the initiator layer, was reduced in the case of high copper (II) to 14.5 ± 2 Å (Γ_{poly} = 0.06 ± 0.03 mg/m^2), compared to 95 ± 10 Å (Γ_{poly} = 1.20 ± 0.15 mg/m^2) for the same conditions but using the usual copper (I) to copper (II) ratio. This confirms that the observed layer formation occurs by ATRP of poly(METAC).

Using similar X-ray reflectometry measurements, we were able to determine how the amount of poly(METAC) varied with the conditions under which the mica was initiator-functionalized. Two otherwise identical samples were prepared with (d = 270 ± 10 Å, Γ_{poly} = 3.65 ± 0.15 mg/m^2) and without (d = 85 ± 10 Å, Γ_{poly} = 1.05 ± 0.15 mg/m^2) Ar/H_2O plasma treatment; the much greater thickness of the former layer shows that Ar/H_2O plasma treatment has a beneficial effect on the coverage and/or stability of the silane initiator layer. This could be due to covalent bonding of silane molecules to surface –OH groups introduced by the plasma [39]. The dependence of poly(METAC) layer thickness on the incubation time in the silane initiator/hexane vapour, t_{inc}, was also examined (figure 2c, polymerization conditions identical for all three samples). The dry poly(METAC) layer thickness increased with the incubation time, presumably because the coverage of silane initiator on the surface increased, but did not reach a plateau before at least 30 hours, suggesting that the silane initiator layer takes at least this long to reach saturated coverage.

For the SFB experiments, we chose an incubation time of 1 hour (Γ_{poly} = 0.53 ± 0.14 mg/m^2, from the data of figure 2c) in the hope that using this quite low polymer grafting density would enable the observation of a regime where the counterions to a polyelectrolyte brush are not fully confined within the brush. It will be seen below that we did indeed observe such a regime.

Control experiments

In order to characterize the polyelectrolyte layer synthesis procedure, forces in water between plasma-treated mica surfaces and between silane-initiated mica surfaces were measured using the SFB. Figure 3a shows the normal forces in pure water between mica surfaces that were treated with an Ar/H_2O plasma as described in the 'Experimental section'. The surfaces experienced a long range repulsion consistent with the presence of an electrical double layer force between the surfaces, which can be fitted with the linearized Poisson-Boltzmann equation [51,58]

$$F(D)/R = \frac{128\pi k_B T \rho_0}{\kappa} \tanh^2\left(\frac{e\psi_0}{4k_B T}\right)\exp(-\kappa D), \qquad (2)$$

where $F(D)$ is the force, R is the radius of curvature, k_B is the Boltzmann constant, ρ_0 is the background number density of 1:1 electrolyte, ψ_0 is the surface potential (assumed constant), and κ^{-1} is the Debye length, defined by [59]

$$\kappa^2 = \frac{2\rho_0 e^2}{\varepsilon\varepsilon_0 k_B T}. \qquad (3)$$

The obtained fitting parameters are ψ_0 = 130 mV and $\rho_0 = 3 \times 10^{-5}$ M. The value of ρ_0 is within the range of literature values reported for SFB experiments in nominally ultrapure water, and may arise from residual ions leached from the glassware and dissolved carbon dioxide from the air [54]. When the surfaces were brought close together ($D \leq 7^{+3}_{-0}$ nm), they jumped spontaneously into adhesive contact, with an interfacial energy $\gamma \geq 3.2$ mJ/m^2 (calculated from the pull-off force, $F_{pulloff}$, using the Johnson-Kendall-Roberts (JKR) theory [51],

according to which $\gamma = F_{pulloff} / 3\pi R$). The values of ψ_0 and γ are similar to those typically observed for mica that has not been plasma treated [17, 60, 61], showing that the charge and roughness of the mica surface have not been significantly altered by the plasma treatment. Shear forces between plasma treated surfaces were measured during the jump in to adhesive contact, and showed no significant coupling between the mica surfaces prior to adhesive contact.

Figure 3b shows normal forces between mica surfaces that had been coated with silane initiator following plasma treatment (mica-vapor reaction time 1 hour). The surfaces experienced a long-range exponentially decaying repulsion presumably arising from an electrical double layer, with a decay length corresponding to a plausible background 1:1 electrolyte concentration of 4×10^{-5} M, followed by a jump into adhesive contact. The jump indicates that the surfaces were free from contamination. The presence of the electrical double layer force indicates that the mica surface retained some negative charge after the silanization process.

Normal forces in pure water

The measured normal forces in water between mica surfaces bearing poly(METAC) brushes are shown in figure 4, with 4a, 4b and 4c representing results from different experiments and contact positions. A typical force profile from figure 4a is shown on figures 4b and 4c; it can be seen that similar results were obtained across different contact positions and experiments, showing that the surface functionalization and brush growth procedures produced largely homogeneous and reproducible surfaces. The force profiles show a long-range exponentially-decaying force which may be attributed to an electrical double layer interaction, since it has an appropriate decay length (corresponding to a background 1:1 electrolyte concentration of order 10^{-5} M), and disappears on the addition of 10^{-2} M 1:1 electrolyte (see below). Exponential fits to this electrical double layer force are shown by the solid and dotted lines in figure 4. At smaller surface separations there is a more rapidly-increasing force, which may be attributed to

the compression of the poly(METAC) brushes, after they have come into contact and which we will refer to as the '*steric'* force.

The forces between polyelectrolyte brushes have been modeled theoretically [24, 62, 63]. Pincus [62] describes two limiting regimes for brushes in pure water: the *osmotic regime*, where the brush is sufficiently dense and highly-charged that all its counterions are confined within it, and the so-called *Pincus regime*, which occurs for less dense or less highly-charged brushes, where the counterions extend far beyond the brush, with the counterion decay length away from the surface being much greater than the brush height. The presence of significant long range electrical double layer forces in figure 4 shows that the counterions in our system extended some way beyond the brush, so that our system shows an important qualitative feature of the Pincus regime. However, the full conditions for the Pincus regime are not fulfilled since the measured Debye length is only about twice the brush height, and the quantitative predictions associated with this regime will therefore not apply.

Importantly, the measured electrical double layer repulsion can be shown to have arisen from the electrical charge of the poly(METAC) layers, and not from any residual charge on the mica surfaces. This is because the magnitude of the measured electrical double layer force is too large for the force to have arisen from repulsion between charged planes situated at the mica surfaces. It can be seen from equation (2) that, if the electrical double layer force between two charged surfaces separated by a distance D is written $F(D)/R = A\exp(-\kappa D)$, then the prefactor A cannot exceed a value $A_{\max} = 128\pi k_B T\rho_0/\kappa$. Since, for the data of figure 4, $A > A_{max}$, the electrical double layer force must arise from repulsion between electrical charges that lie above the mica surface, i.e. from the electrical charge on the polyelectrolyte. We can estimate the position of a nominal plane of charge, although the real charge on the polyelectrolyte is, of course, not located in a single plane. Assuming $e\psi_0 >> 4k_B T$, the nominal planes of charge can be shown to be located a distance $\delta L_{charge} = (1/2\kappa)\ln(A/A_{\max})$ above each mica surface. The data of figure 4 give an average value of δL_{charge} = 22 ± 14 nm,

which is less than the polyelectrolyte layer thickness as measured by the onset of the steric forces, further confirming our identification of the electrical double layer force with the charge on the polyelectrolyte.

To attempt to determine the structure of the brushes studied, the fitted long range exponential forces, extrapolated back to the apparent onset of the steric forces, were subtracted from the measured forces, leaving the steric forces. The steric forces thus determined are shown in figure 5. It can be seen that the steric force increases rapidly from an onset distance of around 60 ± 10 nm, which may be taken to be twice the height of the polyelectrolyte layers. The hysteresis between approaching and receding curves is small in comparison to the total normal force, showing that any attractive forces between the extended polymer chains and the substrate surface are small in comparison with the repulsive force. This indicates that the poly(METAC) layer is better thought of as a polyelectrolyte brush than as a layer of adsorbed polymer. The small hysteresis that does occur could arise from bridging effects due to the partial adsorption of polymer molecules to the opposite surfaces during interpenetration of the polymer layers, or from the compression-induced adsorption of polymer molecules to their own anchoring surfaces. The significant observed shear forces (see "Shear forces" below) indicate that at least part of the normal force hysteresis is likely to derive from bridging effects.

In order to obtain a greater understanding of the data of figure 5, we can compare them with a simple scaling model of polyelectrolyte brushes, first developed by Pincus [62]. This model assumes that brush behaviour is determined by the balance of the osmotic pressure due to trapped counterions, which tends to swell the brush, with the entropic elasticity of the polymer chains, which tends to shrink it. The interaction free energy between the surfaces, *W(D)*, is then given by $W(D) \cong 2\int_{L_0}^{D/2} dL\left(f_{osm}(L) + f_{el}(L)\right)$, where $f_{osm} \cong \left(\alpha N / Ls^2\right)k_B T$ is the osmotic force and $f_{el} \cong \left(L / Na^2 s^2\right)k_B T$ is the elastic force, where L is the brush height, s is the spacing between adjacent anchored chain ends, N is the degree of polymerization, a is the Kuhn step

length, α is the fraction of monomers that are charged and the symbol $\cong$ means equal to within an unknown prefactor of order unity (see Balastre *et al.* for a detailed discussion [24]). The parameter L_0 is the uncompressed height of a brush that contains all its counterions, and is given by [24] $L_0 \cong \alpha^{1/2} Na$. Using the Derjaguin approximation (1), the force between two opposing brushes on curved surfaces is:

$$F(D)/R = Bg\left(\frac{D}{2L_0}\right), \qquad (4)$$

where $g(x) = \gamma_1\left(x^2 - 1\right) - \gamma_2 \ln x$, where γ_1, γ_2 are constants of order unity, and $B = 2\pi\alpha k_B TN / s^2$. $B/2\pi k_B T$ is equal to within an order of magnitude to the number of charged monomers per unit area. γ_1, γ_2 can in theory each take any value of order unity, however, equation (4) is unphysical unless $\gamma_2 \geq 2\gamma_1$ (see appendix).

The solid lines in figure 5 show fits to the measured steric forces using equation (4). Only force profiles measured with the surfaces approaching one another were used for the fitting. In making the fits, emphasis was placed on fitting the data between F/R = 1 mN/m and 10 mN/m. The average value of L_0, obtained from this fitting was 30 ± 8 nm.

We estimate the polydispersity in our polyelectrolyte layer from literature values to be in range M_n/M_w = 1.2 – 1.5 [33]. Such a polydispersity should lead to a slower decay of the steric force at high distances than predicted by the scaling model, due to the tendency of longer polymer chains to extend further away from the substrate surface. It can be seen from figure 5 that this expected deviation of the scaling theory fits away from the measured data does indeed occur.

Fitting with the scaling theory gives values of L_0, and of B, which can be used to collapse all force profiles onto a single curve, confirming their common shape. Defining $y = (F/R)/B$, $x = D/2L_0$, equation (4) can be written $y = g(x)$, with *g(x)* defined as before. Figure 6 shows the approaching steric force profiles from figure 5, plotted as *(F/R)/B*

versus $D/2L_0$, and also shows a plot of equation $y = g(x)$. It can be seen that this scaling process does indeed collapse all force profiles onto a common curve.

We now estimate the degree of polymerization, N, and the spacing between adjacent polymer chain anchor points, s, from the value of L_0 obtained from fitting and the total amount of polymer per unit area obtained from X-ray measurements on the dry brush (see "Dry brush characterization"). From the scaling theory expression $L_0 \cong \alpha^{1/2} N a$ [64], we obtain $N = 120 \pm 30$ and $s = 9 \pm 2.5$ nm, estimating the Kuhn step length a from literature light scattering data. Recalling that $L_0 = 30 \pm 8$ nm, this estimate is consistent with the idea that adjacent polymer chains are overlapping, and the system is indeed in a brush-like, rather than a mushroom-like regime.

Normal forces with added electrolyte

We now describe measurements of the normal forces between mica surfaces bearing poly(METAC) brushes in aqueous solutions of sodium nitrate. Nitrate ions were used as these are known to screen the charges, but do not introduce counterion-specific effects such as have been observed in some other systems [30, 65-67]. After the normal force profiles in pure water shown in figure 4b had been measured, some of the water was removed from the SFB and replaced with an aqueous solution of sodium nitrate, giving an overall concentration of sodium nitrate in the SFB of $1.50^{+0.3}_{-0.2} \times 10^{-2}$ M. Normal force profiles were then measured. Subsequently, the procedure was repeated using a more concentrated solution, raising the concentration to $1.22^{+0.18}_{-0.14} \times 10^{-1}$ M.

The measured normal force profiles in 1.50×10^{-2} M and 1.22×10^{-1} M solutions were essentially identical, and are shown in figure 7. The long-range force that was present in pure water was not visible in these profiles, as can be seen by comparaison with the representative pure water force profile shown (dashed line in figure 7, data from figure 4a). This helps to confirm that the long-range force in pure water arose from an electrical double layer, since

electrical double layer forces fall off rapidly with distance at such high electrolyte concentrations, as can be seen from equations (2) and (3).

Figure 7 also shows the steric forces in pure water at the same contact position as the electrolyte measurements (data from figure 5a, shown by hatched area between dotted lines to allow for scatter). The forces in electrolyte solution are lower than the steric forces in pure water for any given surface separation, D, down to roughly D = 5 – 10 nm. This suggests that the brush has contracted on the addition of electrolyte, which is in accordance with theoretical expectations, since the range of electrostatic interactions decreases due to screening effects at high electrolyte concentrations, and with previous observations [24, 30, 68, 69]. The observed contraction is greater in the outer part of the brush. This is as expected, since the outer part of the brush must have a lower density of monomers and thus of counterions, and strong contraction is predicted to occur only when the electrolyte concentration is equal to or greater than the counterion concentration [62]. No significant further contraction is observable following the increase of the electrolyte concentration from ~10^{-2} M to ~10^{-1} M.

Shear forces

Shear force measurements were carried out immediately after the first approaching normal force profile shown in figure 4b with the surfaces still close together. A typical shear force trace is shown in figure 8. The top surface is moved parallel to the bottom surface, so that the lateral displacement of the top surface follows a triangular wave. When the displacement is small, the bottom surface is rigidly coupled to the top surface and so moves along with it, deflecting the SFB lateral springs (see 'Experimental section'), in response to the shear force between the surfaces. When this force becomes great enough, the surfaces begin to slide past one another, during which time the shear force is constant; the value of this constant force is known as the 'sliding friction', F_s. When the direction of the applied motion is reversed, the process repeats itself.

Figure 9a shows the sliding friction as a function of the applied shear rate $\dot{\gamma} = v_{appl} / D$, where v_{appl} is the applied speed of lateral motion of the top surface, and D = 3 ± 1 nm throughout these measurements. The measured forces are of order 10 μN, and increase slowly with the shear rate. These frictional forces could plausibly arise from bridging between the surfaces, arising from the adhesive forces between the surfaces the presence of which is suggested by the observed hysteresis in the normal force profiles (see 'Normal forces in pure water'). These adhesive forces are likely to be electrostatic attractions between the poly(METAC) and the oppositely-charged surface and/or hydrophobic attractions between the silane initiator surface and the poly(METAC) backbone. The sliding shear stress is of order 10^4 Pa; this was estimated by using the Hertz model of nonadhesive contact between elastic bodies to estimate the contact area, and assuming an elastic modulus for the mica-glue combination of order 10^9 Pa [70].

The increase in shear force at increased applied shear rate can be understood, if the forces do arise from bridging, by considering the 'breaking' of a bridge by desorption of the polymer chain from the opposite surface as a stochastic event that, in the absence of an applied shear stress, would require a potential barrier to be overcome by thermal fluctuations. The application of a shear stress reduces the potential barrier for bridge breaking, and thus reduces the typical timescale on which it occurs. The faster the surfaces are slid past one another, the shorter the timescale on which bridges must be broken, and so the higher the shear stress, in accordance with figure 9. Similar ideas have been pursued quantitatively, giving an expression for the shear force of the form [71] $F_{shear} = W + X \ln \dot{\gamma}$. Figure 9b shows a log-linear plot of shear force vs. shear rate, with a fit to this equation. The measured shear forces are consistent with this model, helping to confirm that bridging may indeed be the explanation for the observed friction.

Despite bridging effects, the polyelectrolyte layers still provided some lubricating effect at high surface separations. Subsequent measurements (not shown) suggest that the shear force

was below readily detectable levels (i.e. below about 1 μN) down to around D = 30-40 nm, significantly after the brushes came into contact (D = 60 – 70 nm). The shear force is in general likely to be highly dependent on the grafting density of the polyelectrolyte layer.

One of the original aims of this investigation was to produce brush-like polyelectrolyte layers that were sufficiently strongly bound to the mica surface to allow SFB studies of friction at high compression; it can be seen from the measurements just described that this has been achieved. The subsequently measured normal force profiles (figure 4a) confirm that no significant amounts of polymer were removed from the surface as a result of shearing at high compressions, since the normal forces at high compressions, which are a good indicator of the amount of polymer on the surfaces, were similar before and after shearing. It is thus clear that the surface-grown polyelectrolyte brushes described in this paper represent a qualitative improvement in terms of mechanical stability on the diblock brushes used in a previous study of polyelectrolyte brush friction [17].

Conclusions

We have measured normal and shear forces between mica surfaces bearing polyelectrolyte layers that were synthesized from the surface by ATRP.

Normal force measurements revealed a long-range electrical double-layer force, and a shorter-range steric force that could be fitted with the Pincus theory [24, 62]. Upon addition of sodium nitrate at concentrations of up to 10^{-1} M, screening effects reduced the long-range electrical double layer force to an undetectable level.

Measurements of shear forces between the polyelectrolyte layers showed sliding friction with sliding shear stresses of order 10^4 Pa. These frictional forces could plausibly arise from the presence in our system of adhesive bridging forces between the surfaces in our system, which is suggested by a slight hysteresis in the normal force profiles. The poly(METAC) layers withstood shear at high compressions without large amounts of polymer being removed

from the surface, emphasizing the potential advantages of polyelectrolyte layers that have been synthesized from the surface.

Acknowledgements

We thank Robert K. Thomas, Frank Schreiber and Richard Jones for useful discussions. We acknowledge financial support from EPSRC (IED, WHB, JK), the Petroleum Research Fund (grant 45964-AC7) (JK), the Charles McCutchen Foundation (JK), the Israel Science Foundation (JK), the Minerva Foundation (JK), a Royal Society University Research Fellowship (ST), and a Corpus Christi College, Oxford Senior Scholarship (IED).

Appendix: Scaling prefactors in equation (4)

This appendix describes why equation (4) [24],

$$F(D)/R = Bg\left(\frac{D}{2L_0}\right), \tag{A.1}$$

where

$$g(x) = \gamma_1\left(x^2 - 1\right) - \gamma_2 \ln x, \tag{A.2}$$

results in physically meaningful forms for *F(D)* only when $\gamma_2 \geq 2\gamma_1$. (Recall that γ_1 and γ_2 can in theory take any value of order unity.)

For *F(D)* to be physical, *g(x)* must fall monotonically to zero at $x = 1$, when the brushes disengage from each other. The value of *g(x)* for $x > 1$ is not important, as in this regime, the force is zero and is no longer given by equation (A.1). Note that *g(x)* has been deliberately constructed so that *g(x*=1*)* is equal to zero for all values of γ_1 and γ_2. However, it turns out that for certain values of γ_1 and γ_2, *g(x)* does not monotonically decrease for $x < 1$.

As *g(x)* is the sum of a monotonically increasing and a monotonically decreasing function, it must have a single stationary point. Since *g(x)* is large and positive in the limits $x \to 0$ and $x \to \infty$, the single stationary point must be a minimum. There are then three possible

scenarios, depending on the values of γ_1 and γ_2. Let $\bar{x}$ be the value of x when $g(x)$ is at a minimum. If $\bar{x} < 1$, then $g(x) = 0$ has a root for $x < 1$, as well as the omnipresent root at $x = 1$. If $\bar{x} = 1$, then $g(x) = 0$ has two repeated roots at $x = 1$. Finally, if $\bar{x} > 1$, then $g(x)$ has a root at $x = 1$ and one at $x > 1$ only. The first two of these scenarios are physically acceptable, whilst the scenario $\bar{x} < 0$ is not, since $g(x)$ falls unphysically to zero and beyond for $x < 1$. To obtain a physically acceptable $g(x)$, we must thus choose γ_1 and γ_2 such that $\bar{x} \geq 1$.

Setting $\left(dg/dx\right)_{x=\bar{x}} = 0$, we find that

$$\bar{x} = \sqrt{\frac{\gamma_2}{2\gamma_1}} \tag{A.3}$$

so that to obtain $\bar{x} > 1$, we require

$$\gamma_2 \geq 2\gamma_1 . \tag{A.4}$$

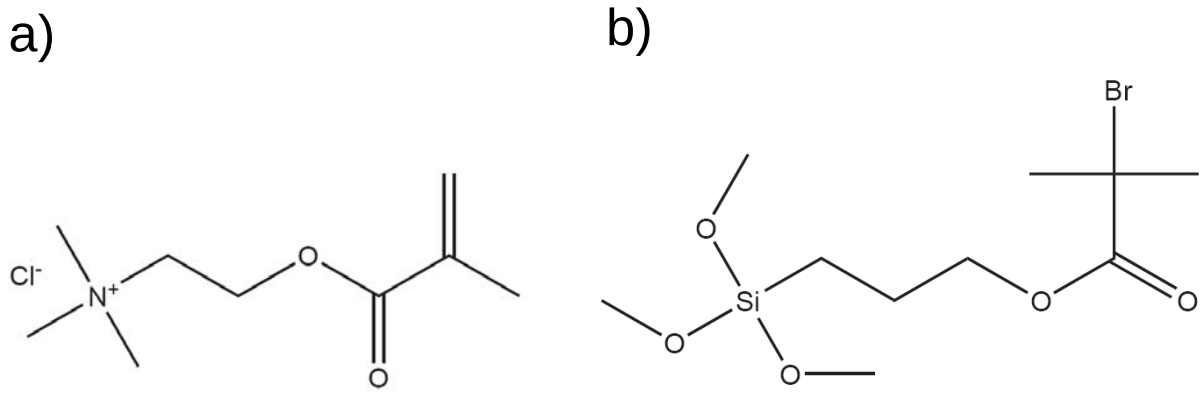

Figure 1. The structures of a) [2-(methacryoyloxy)ethyl]trimethylammonium chloride (METAC) (polymerization is about the C=C double bond) b) 3-trimethoxysilylpropyl-2-bromo-2-methylpropionate (silane initiator).

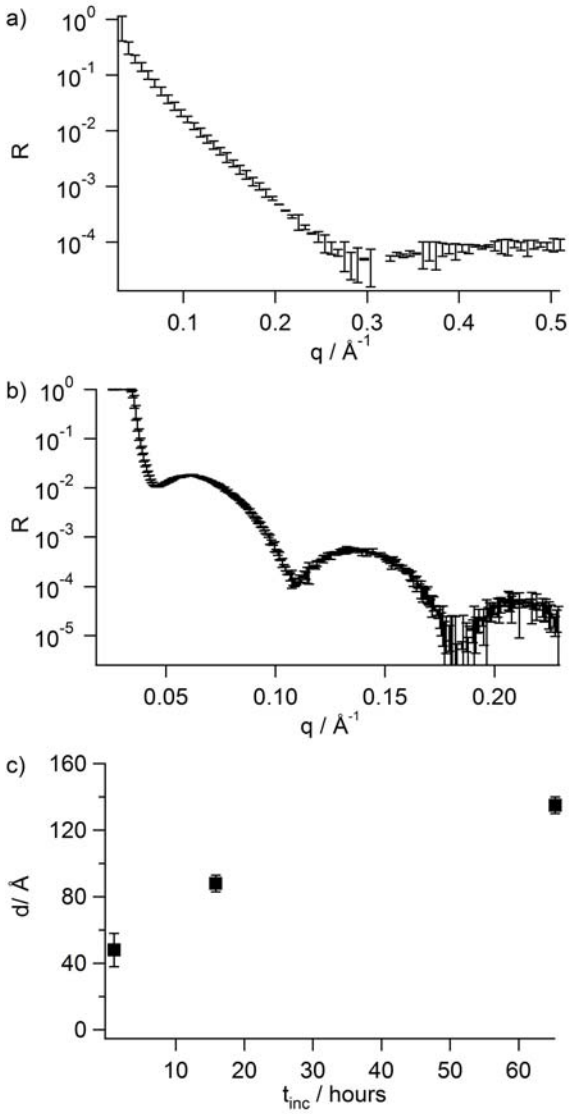

Figure 2. a) X-ray reflectivity from a silane initiator-functionalized mica surface: reflectivity, *R*, vs. momentum transfer, *q*. b) X-ray reflectivity from a mica surface on which a poly(METAC) brush has been grown from a silane initiator layer. Kiessig fringe are visible in both cases. c) The effect of the incubation time, t_{inc}, of the mica in the silane initiator/hexane vapour on the polymer layer 'dry' thickness, *d*, measured using X-ray reflectometry. Error bars represent the uncertainty in the fitting. The point at around 15 hours is derived from the reflectivity profile shown in (b).

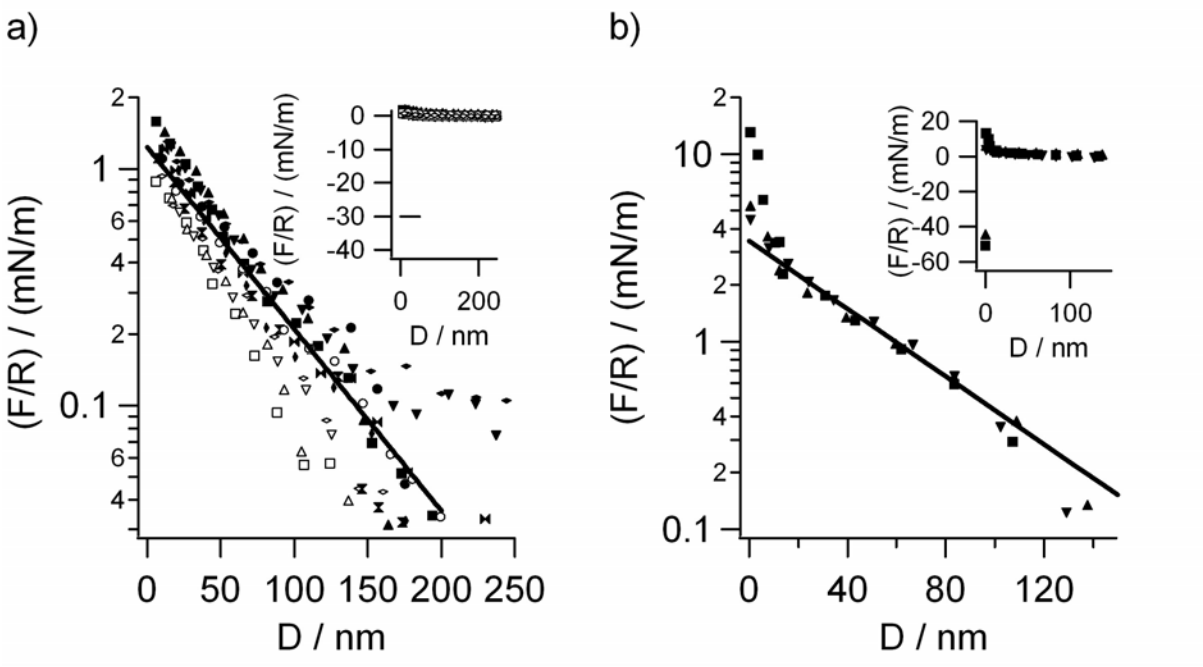

Figure 3. SFB control experiments. a) Normal forces in water between mica surfaces that have been treated with an Ar/H_2O plasma. Filled (■, ▲, ▼, ●, ◆, ♦, ⋈, ⧗) and open (□, △, ▽, ○, ◇) symbols respectively indicate force profiles measured at two different contact positions. The solid line shows a fit to equation (2), with ψ_0 = 130 mV and κ given by equation (3) with $\rho_0 = 3 \times 10^{-5}$ M. b) Normal forces in water between mica surfaces bearing a silane initiator layer. Symbols show measured force profiles, in chronological order: ■, ▲, ▼. The solid line shows an exponential fit with the slope κ given by equation (3) with $\rho_0 = 4 \times 10^{-5}$ M. Insets show the same force profiles as the main graphs, on linear scales, so that the jump into adhesive contact can be seen. Inset to a): the measured lower limit on the magnitude of the pull-off force was 30 mN/m, marked by the solid line.

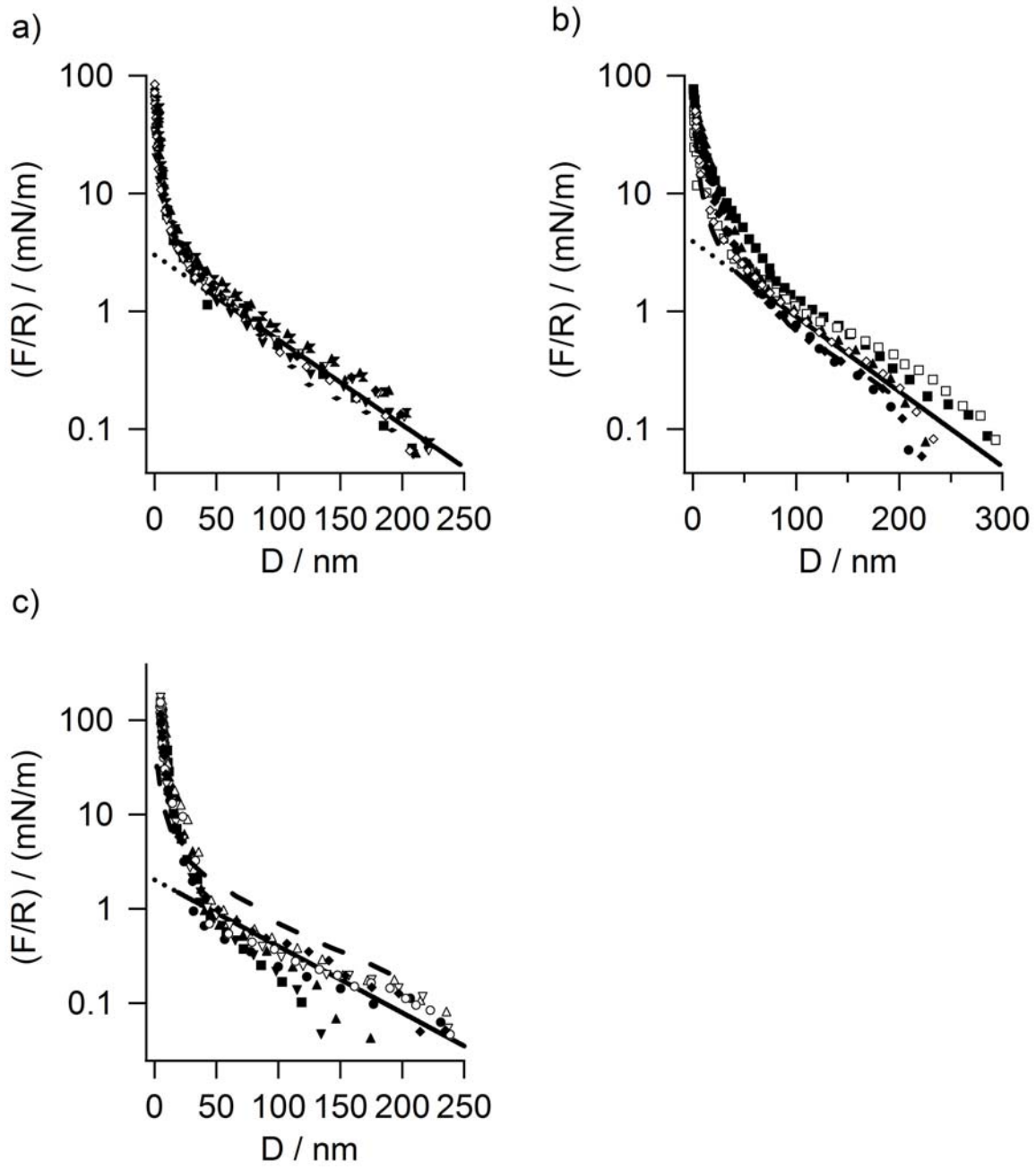

Figure 4. Normal forces in water between surface-grown poly(METAC) brushes. Filled symbols show approaching and open symbols receding force profiles, from different contact positions within a given experiment (a), b)) and from a second experiment (c)) Symbols show measured force profiles in chronological order for each sub-figure: a) ■, ▲, ▼, ▽, ◆, ◇, ⬧, ⬨, ⧗, b) ■, □, ▲, ●, ◆, ◇, c) ■, ▲, △, ▼, ▽, ●, ○, ◆. Solid lines show fits to equation (2) with the following values: a) $\kappa^{-1} = 60^{+4}_{-3}$ nm, giving $\rho_0 = 2.5 \pm 0.3 \times 10^{-5}$ M, b) $\kappa^{-1} = 68^{+6}_{-5}$ nm, giving $\rho_0 = 2.0 \pm 0.3 \times 10^{-5}$ M, c) $\kappa^{-1} = 62^{+8}_{-6}$ nm, giving $\rho_0 = 2.4^{+0.6}_{-0.5} \times 10^{-5}$ M. Dotted lines

show extrapolations of fits below $D = 2\delta L_{charge}$ as a guide to the eye. Dashed lines in b) and c) show a typical force profile from (a) for comparison (▲ from (a)).

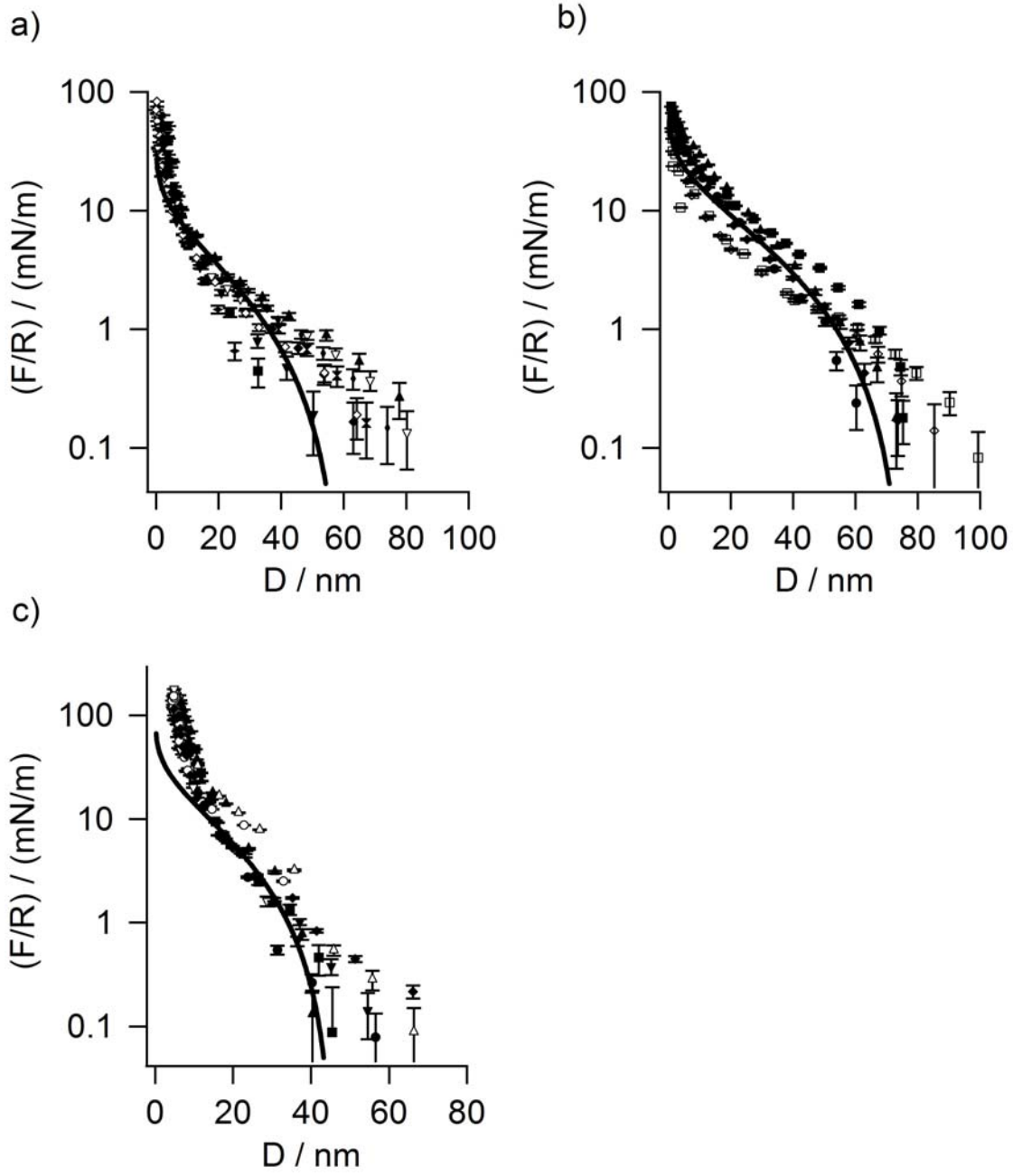

Figure 5. 'Steric' normal forces between mica surfaces bearing surface-grown poly(METAC) brushes. Symbols show the same force profiles as in figure 4, but with the long-range electrical double layer force removed as described in the text. The indicated errors arise from the uncertainty in the force onset distance. The solid line show fits to equation (4), with γ_1 = 0.75, γ_2 = 1.50 and: a) B = 3.5 mN/m, $2L_0$ = 60 nm, b) B = 7.0 mN/m, $2L_0$ = 76 nm, c) B = 9.0

mN/m, $2L_0$ = 46 nm. The electrical double layer force was fitted and subtracted separately for each measured force profile.

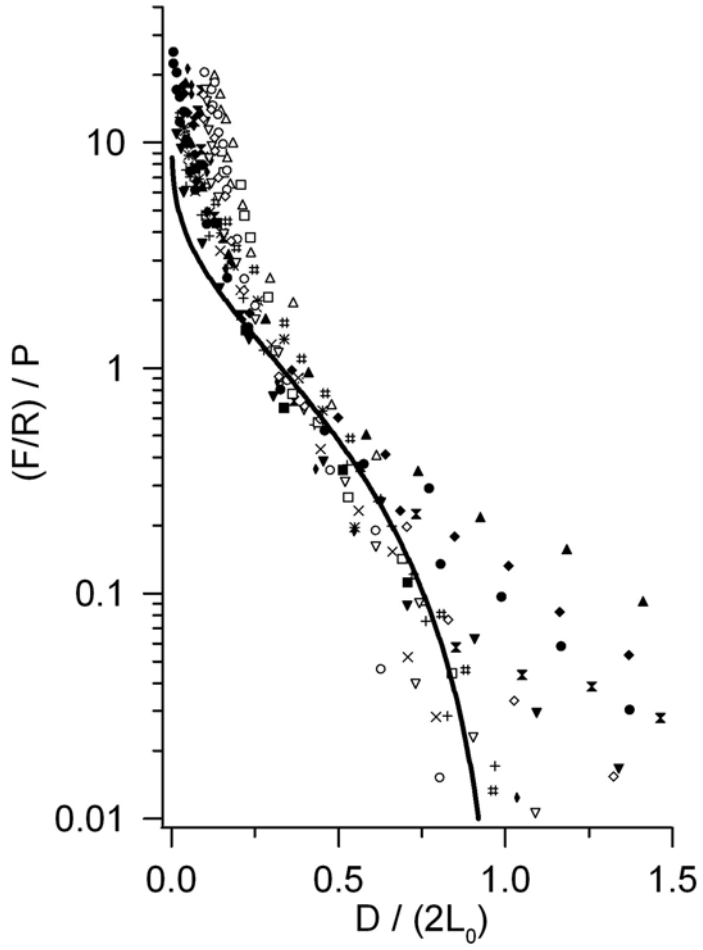

Figure 6. 'Steric' normal forces in water between mica surfaces bearing surface-grown poly(METAC) brushes, plotted in terms of the dimensionless variables $(F/R) / P$ and $D / 2L_0$, where P and L_0 were determined for each experiment or contact position by the fits shown in figure 5. 'Steric' force profiles from different experiments and contact positions are thus collapsed onto a universal curve. Approaching force profiles are shown, with data taken from figure 5a) ■, ▲, ▼, ●, ◆, ♦, ⧗, 5b) #, *, ×, +, 5c) □, △, ▽, ○, ◇ . The solid line is a plot of $y = g(x)$ as described in the text, with $\gamma_1 = 0.75$, $\gamma_2 = 1.50$.

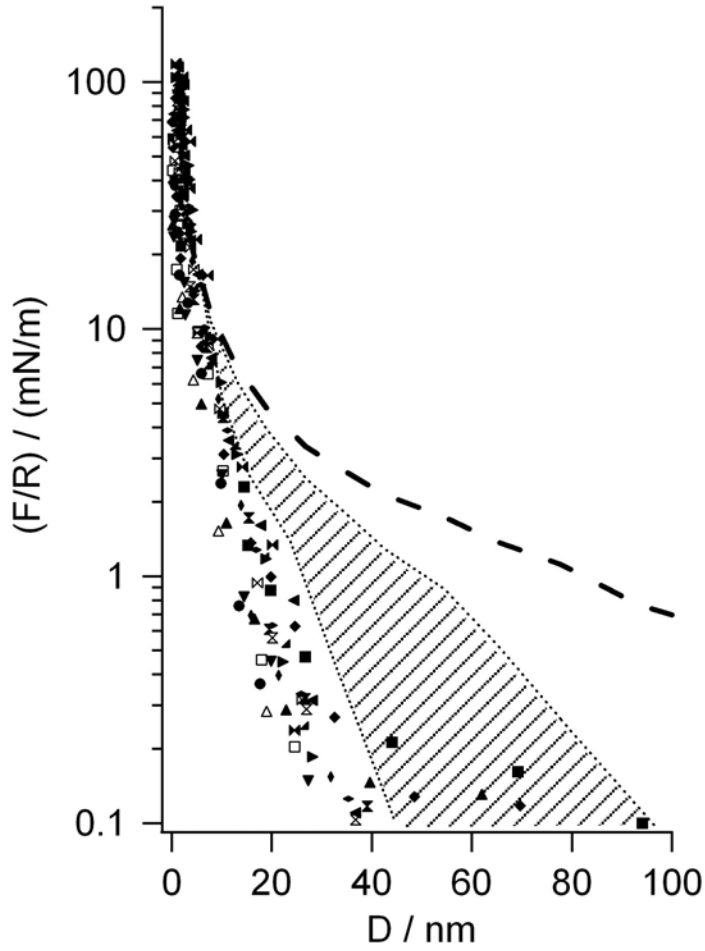

Figure 7. Normal forces between surface-grown poly(METAC) brushes in electrolyte solutions. Filled symbols show approaching and open symbols receding force profiles, measured in $1.5^{+0.3}_{-0.2} \times 10^{-2}$ M (■, □, ▲, △, ▼, ⬢, ◆, ⧫, ➧) and $1.22^{+0.18}_{-0.14} \times 10^{-1}$ M (⧓, ⋈, ⧗, ⧖, ◀, ▶, ◢) aqueous solutions of sodium nitrate. For comparison, the dashed line (----) shows a normal force profile in pure water (▲ from figure 4a) and the hatched area between dotted lines (····) shows the approximate area within which the steric force profiles lie (figure 5a) (all force profiles shown were measured at the same contact position).

Figure 8. Typical shear forces in water between mica surfaces bearing surface-grown poly(METAC) brushes, measured immediately after the first approaching normal force profile shown in figure 4b, at $D = 3 \pm 1$ nm. a) The applied relative displacement of the surfaces (right axis): a triangular wave with peak to peak distance 0.5 µm. b) The resultant shear force (left axis). The magnitude of the sliding friction between the surfaces is given by the plateau height F_s. The timescale is the same in a) and b).

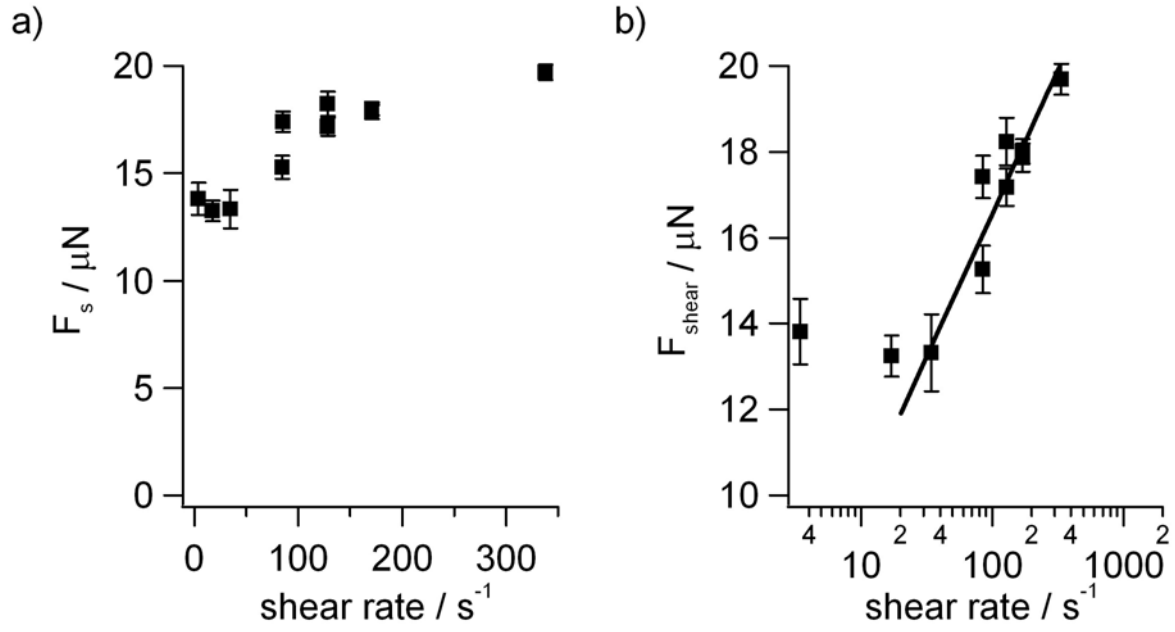

Figure 9. Sliding friction in water as a function of shear rate for mica surfaces bearing surface-grown poly(METAC) brushes. Measurements taken at D = 3 ± 1 nm, measured immediately after the first approaching normal force profile shown in figure 4b with F_s determined as shown in figure 8. The same data are plotted on a) linear-linear and b) log-linear axes. The solid line in b) shows a theoretical fit as described in the text.

References

1. Klein, J.; Kumacheva, E.; Mahalu, D.; Perahia, D.; Fetters, L. J. Nature 1994, 370, (6491), 634-636.

2. Kilbey, S. M.; Bates, F. S.; Tirrell, M.; Yoshizawa, H.; Hill, R.; Israelachvili, J. Macromolecules 1995, 28, (16), 5626-5631.

3. Muller, M. T.; Yan, X. P.; Lee, S. W.; Perry, S. S.; Spencer, N. D. Macromolecules 2005, 38, (13), 5706-5713.

4. Muller, M. T.; Yan, X. P.; Lee, S. W.; Perry, S. S.; Spencer, N. D. Macromolecules 2005, 38, (9), 3861-3866.

5. Klein, J. Annual Review of Materials Science 1996, 26, 581-612.

6. Witten, T. A.; Leibler, L.; Pincus, P. A. Macromolecules 1990, 23, (3), 824-829.

7. Wijmans, C. M.; Zhulina, E. B.; Fleer, G. J. Macromolecules 1994, 27, (12), 3238-3248.

8. Klein, J. Proceedings of the Institution of Mechanical Engineers, Part J: Journal of Engineering Tribology 2006, In press.

9. Ligtenberg, M. J. L.; Buijs, F.; Vos, H. L.; Hilkens, J. Cancer Research 1992, 52, (8), 2318-2324.

10. Carraway, K. L.; Fregien, N.; Carraway, K. L.; Carraway, C. A. C. Journal of Cell Science 1992, 103, 299-307.

11. Argueso, P.; Spurr-Michaud, S.; Russo, C. L.; Tisdale, A.; Gipson, I. K. Investigative Ophthalmology & Visual Science 2003, 44, (6), 2487-2495.

12. Komatsu, M.; Carraway, C. A. C.; Fregien, N. L.; Carraway, K. L. Journal of Biological Chemistry 1997, 272, (52), 33245-33254.

13. Dhinojwala, A.; Cai, L.; Granick, S. Langmuir 1996, 12, (19), 4537-4542.

14. Schorr, P. A.; Kwan, T. C. B.; Kilbey, S. M.; Shaqfeh, E. S. G.; Tirrell, M. Macromolecules 2003, 36, (2), 389-398.

15. Tadmor, R.; Janik, J.; Klein, J.; Fetters, L. J. Physical Review Letters 2003, 91, (11), -.

16. Raviv, U.; Frey, J.; Sak, R.; Laurat, P.; Tadmor, R.; Klein, J. Langmuir 2002, 18, (20), 7482-7495.

17. Raviv, U.; Giasson, S.; Kampf, N.; Gohy, J. F.; Jerome, R.; Klein, J. Nature 2003, 425, (6954), 163-165.

18. Kampf, N.; Gohy, J. F.; Jerome, R.; Klein, J. Journal of Polymer Science Part B-Polymer Physics 2005, 43, (2), 193-204.

19. Benz, M.; Chen, N. H.; Israelachvili, J. Journal of Biomedical Materials Research Part A 2004, 71A, (1), 6-15.

20. Liberelle, B.; Giasson, S. Langmuir 2008, 24, (4), 1550-1559.

21. Sokoloff, J. B. (Unpublished) 2008.

22. Raviv, U.; Klein, J. Science 2002, 297, (5586), 1540-1543.

23. Briscoe, W. H.; Titmuss, S.; Tiberg, F.; Thomas, R. K.; McGillivray, D. J.; Klein, J. Nature 2006, 444, 191-194.

24. Balastre, M.; Li, F.; Schorr, P.; Yang, J. C.; Mays, J. W.; Tirrell, M. V. Macromolecules 2002, 35, (25), 9480-9486.

25. Abraham, T.; Giasson, S.; Gohy, J. F.; Jerome, R. Langmuir 2000, 16, (9), 4286-4292.

26. Li, F.; Balastre, M.; Schorr, P.; Argillier, J. F.; Yang, J. C.; Mays, J. W.; Tirrell, M. Langmuir 2006, 22, (9), 4084-4091.

27. Ligoure, C.; Leibler, L. Journal De Physique 1990, 51, (12), 1313-1328.

28. Dunlop, I. E.; Briscoe, W. H.; Titmuss, S.; Sakellariou, G.; Hadjichristidis, N.; Klein, J. Macromolecular Chemistry and Physics 2004, 205, (18), 2443-2450.

29. Titmuss, S.; Briscoe, W. H.; Dunlop, I. E.; Sakellariou, G.; Hadjichristidis, N.; Klein, J. Journal of Chemical Physics 2004, 121, (22), 11408-11419.

30. Biesalski, M.; Johannsmann, D.; Ruhe, J. Journal of Chemical Physics 2004, 120, (18), 8807-8814.

31. Matyjaszewski, K., Chapter 8. In Handbook of radical polymerization, Matyjaszewski, K., Ed. John Wiley and Sons, Inc.: Hoboken, U.S.A., 2002.

32. Ejaz, M.; Yamamoto, S.; Ohno, K.; Tsujii, Y.; Fukuda, T. Macromolecules 1998, 31, (17), 5934-5936.

33. Pyun, J.; Kowalewski, T.; Matyjaszewski, K. Macromolecular Rapid Communications 2003, 24, (18), 1043-1059.

34. Edmondson, S.; Osborne, V. L.; Huck, W. T. S. Chemical Society Reviews 2004, 33, (1), 14-22.

35. Ruhe, J.; Ballauff, M.; Biesalski, M.; Dziezok, P.; Grohn, F.; Johannsmann, D.; Houbenov, N.; Hugenberg, N.; Konradi, R.; Minko, S.; Motornov, M.; Netz, R. R.; Schmidt, M.; Seidel, C.; Stamm, M.; Stephan, T.; Usov, D.; Zhang, H. N. Adv. Polymer Sci. 2004, 165, 79-150.

36. Ballauff, M.; Borisov, O. Curr. Opin. Colloid Interface Sci. 2006, 11, (6), 316-323.

37. Kim, S.; Christenson, H. K.; Curry, J. E. Langmuir 2002, 18, (6), 2125-2129.

38. Ruths, M.; Johannsmann, D.; Ruhe, J.; Knoll, W. Macromolecules 2000, 33, (10), 3860-3870.

39. Kim, S.; Christenson, H. K.; Curry, J. E. Journal of Physical Chemistry B 2003, 107, (16), 3774-3781.

40. Parker, J. L.; Cho, D. L.; Claesson, P. M. Journal of Physical Chemistry 1989, 93, (16), 6121-6125.

41. Wood, J.; Sharma, R. Langmuir 1994, 10, (7), 2307-2310.

42. Okusa, H.; Kurihara, K.; Kunitake, T. Langmuir 1994, 10, (10), 3577-3581.

43. Lego, B.; Skene, W. G.; Giasson, S. Langmuir 2008, 24, (2), 379-382.

44. Zhulina, E. B.; Borisov, O. V.; van Male, J.; Leermakers, F. A. M. Langmuir 2001, 17, (4), 1277-1293.

45. Dunlop, I. E.; Thomas, R. K.; Titmuss, S.; Osborne, V. L.; Edmondson, S.; Huck, W. T. S.; Klein, J. In preparation.

46. Osborne, V. L.; Jones, D. M.; Huck, W. T. S. Chemical Communications 2002, (17), 1838-1839.

47. Tsarevsky, N. V.; Pintauer, T.; Matyjaszewski, K. Macromolecules 2004, 37, (26), 9768-9778.

48. Parratt, L. G. Physical Review 1954, 95, (2), 359-369.

49. Parratt32 or the reflectivity tool. http://www.hmi.de/bensc/instrumentation/instrumente/v6/re°/parratt_en.htm#top.

50. Klein, J.; Kumacheva, E. Journal of Chemical Physics 1998, 108, (16), 6996-7009.

51. Israelachvili, N., Intermolecular and surface forces. 2nd ed.; Academic Press: London, U.K., 1992.

52. Raviv, U.; Laurat, P.; Klein, J. Nature 2001, 413, (6851), 51-54.

53. Kohonen, M. M.; Meldrum, F. C.; Christenson, H. K. Langmuir 2003, 19, (3), 975-976.

54. Perkin, S.; Chai, L.; Kampf, N.; Raviv, U.; Briscoe, W.; Dunlop, I.; Titmuss, S.; Seo, M.; Kumacheva, E.; Klein, J. Langmuir 2006, 22, (14), 6142-6152.

55. Raviv, U.; Perkin, S.; Laurat, P.; Klein, J. Langmuir 2004, 20, (13), 5322-5332.

56. 2-bromo-2-methyl-N-(3-(trimethoxysilyl)propyl)propanamide: a silane initiator molecule that is identical to that described apart from the replacement of the oxygen molecule at the initiator end of the propyl chain (Figure 1b) by –NH–, was used for this measurement, as well as in the experiments to determine the effects of copper (II) : copper (I) ratio and plasma treatment described in this section. The change may slightly alter the reactivity of the initiator group, but should not affect the self-assembly properties of the molecule unchanged. (10 µl of amide silane initiator were mixed with 30 ml of hexane, and the incubation time in the dessicator was 24 hours).

57. Exceptionally, this experiment was carried out using the methanol/water and 2,2'-dipyridine system of Osborne et al. The molar ratio of copper (I) chloride to copper (II) chloride was 20:1 for the 'usual' sample, and 1:1 for the 'high copper (II)' sample.)

58. Equation (2) is strictly valid only for low values of the surface potential ψ0, and is thus not valid when A = Amax for practical parameter values (Ref. 49). However, both numerical solution of the full non-linear Poisson-Boltzmann equation and the results of mica SFB measurements (Refs. 57, 58) confirm that the saturation of W(D) predicted by equation (2) is real, and that the value of Amax given by equation (5) is approximately correct. We can thus regard equation (2) as a heuristic model that captures the saturation behaviour.

59. Barrat, J.-L.; Hansen, J.-P., Basic concepts for simple and complex fluids. Cambridge University Press: Cambridge, U.K., 2003.

60. Pashley, R. M. Journal of Colloid and Interface Science 1981, 80, (1), 153-162.

61. Raviv, U.; Laurat, P.; Klein, J. Journal of Chemical Physics 2002, 116, (12), 5167-5172.

62. Pincus, P. Macromolecules 1991, 24, (10), 2912-2919.

63. Miklavic, S. J.; Marcelja, S. Journal of Physical Chemistry 1988, 92, (23), 6718-6722.

64. Aseyev, V. O.; Tenhu, H.; Klenin, S. I. Macromolecules 1998, 31, (22), 7717-7722.

65. Azzaroni, O.; Moya, S.; Farhan, T.; Brown, A. A.; Huck, W. T. S. Macromolecules 2005, 38, (24), 10192-10199.

66. Konradi, R.; Ruhe, J. Macromolecules 2005, 38, (10), 4345-4354.

67. Mei, Y.; Ballauff, M. European Physical Journal E 2005, 16, (3), 341-349.

68. Guo, X.; Ballauff, M. Phys. Rev. E 2001, 6405, (5), -.

69. Tran, Y.; Auroy, P.; Lee, L. T. Macromolecules 1999, 32, (26), 8952-8964.

70. Horn, R. G.; Israelachvili, J. N.; Pribac, F. Journal of Colloid and Interface Science 1987, 115, (2), 480-492.

71. Briscoe, B. J.; Evans, D. C. B. Proceedings of the Royal Society of London Series a-Mathematical Physical and Engineering Sciences 1982, 380, (1779), 389-&.